PERGAMON

Computers & Geosciences 28 (2002) 485–499

COMPUTERS & GEOSCIENCES

www.elsevier.com/locate/cageo

Numerical simulation of the evolution of aquifer porosity and species concentrations during reactive transport ☆

Jui-Sheng Chen[a], Chen-Wuing Liu[b,*]

[a] Department of Environmental Engineering and Sanitation, Foo-Yin Institute of Technology, Kaohsiung, Taiwan, ROC
[b] Department of Agricultural Engineering, National Taiwan University, Taipei, Taiwan, ROC

Received 1 August 2000; received in revised form 5 June 2001; accepted 10 June 2001

Abstract

While flowing through a porous medium, a reactive fluid dissolves minerals thereby increasing its porosity and ultimately the permeability. The reactive fluid flows preferentially into highly permeable zones, which are therefore dissolved most rapidly, producing a further preferential permeability enhancement. Thus, the reaction front may be unstable. However, other factors, such as diffusion, suppress the instability of a reaction front. This study presents a numerical model to evaluate the interactions between mechanisms that determine the shape of a reactive front. That is, a method is developed to solve a set of nonlinear equations coupled with fluid flow, species transport, and rock–fluid reactions and includes the effects of grain dissolution and the alteration of porosity and permeability due to mineral–fluid reactions. The numerical model enables us to evaluate how a dissolution reaction affects the porosity structure and fluid pressure variation, from which local Darcy flux can then be evaluated. In addition, the model is used to examine how upstream pressure gradient affects the morphological instability of the species concentrations and the aquifer porosity. Simulation results indicate that, although stable for small upstream pressure gradients, the growth of a planar front becomes unstable for large upstream ones. Moreover, the diffusive, advective and resultant species fluxes of both these mechanisms are computed and presented to further elucidate the behavior of the morphological instability for a planar concentration and porosity front that results from the interactions between diffusion and advection.

Keywords: Permeability; Evolution; Dissolution; Reactive transport

1. Introduction

In subsurface formations, modeling coupled reactions and flow involve critical geochemical functions in terms of interpreting phenomena such as weathering, diagenesis and ore deposition (Lichtner, 1996). The water–mineral interaction is of relevant interest in several branches of geochemistry that includes subsurface flow and chemical processes. The change in aquifer porosity owing to the interaction of a penetrating fluid with a porous solid has received considerable attention. That is, due to complete rock dissolution, these phenomena can produce dissolution fingers and create flow channels (Liu et al., 1997). When flowing through a porous medium, a reactive fluid dissolves the mineral, thereby increasing porosity and ultimately permeability. Regardless of whether hydraulic or thermal driving forces are maintained, the flow pattern evolves as the permeability distribution changes. The reactive fluid flows preferentially into zones of high permeability, which are subsequently dissolved rapidly, ultimately producing a further preferential permeability enhancement. Thus, the reaction front may be unstable. However, other factors such as diffusion consistently compete with the flow focusing mechanism, which prevents the elongation

☆ Code available from server at http://www.iamg.org/CG-Editor/index.htm.

*Corresponding author. Fax: +886-2-23639557.
E-mail address: lcw@gwater.agec.ntu.edu.tw (C.-W. Liu).

0098-3004/02/$ - see front matter
PII: S0098-3004(01)00084-X

of the finger from proceeding indefinitely. The diffusion effect inhibits nonuniformities of the reaction front, which ultimately produces either a planar or nonplanar reaction front. The instability of reaction fronts has been studied extensively (Chadam et al., 1986). Through an analytical approach, Sherwood (1987) developed a simple model that demonstrates how the Damkőhler number and the acid capacity number affect the instability of a planar reaction front. However, this investigation did not incorporate the porosity variation, which produces variation in microscopic fluid velocity. Hinch and Bhatt (1990) examined the stability of a moving reaction front using the standard of chemical reaction rate proportional to the product of concentration of fluid and soluble minerals. Furthermore, Ortoleva et al. investigated the stability of a moving reaction front (Chadam et al., 1986; Ortoleva et al., 1987a, b). They used complex reaction equations and included solute diffusion as well as significant changes in the porosity. A series of studies, which considered layered porous media (Xin et al., 1993), was performed on the shape stability of a moving reaction front via the perturbation method, in which a moving reactive front for viscosity changes (Chadam et al., 1991). According to their results, a planar dissolution front is unstable and small perturbation to the front may develop into long fingers. Although the linear stability analysis of reactive transport system equations demonstrates the morphological instability of planar fronts, the nonlinear problem must be numerically simulated to understand more thoroughly the dynamics of the reactive fingering problem. Steefel and Lasaga (1990) used two-dimensional simulations to investigate how coupling chemical reactions and fluid flow affect the space–time evolution of rock dissolution patterns. Lichtner (1992) developed a system of reactive transport equations based on continuum approach and applied to study supergene copper enrichment and metasomatic zoning (Lichtner and Biino, 1992; Lichtner and Balashov, 1993). Chen and Ortoleva (1990) used a computer code to predict the temporal evolution of the reactive feedback problem. Recently, Liu et al. (1997) proposed a geochemical simulator that coupled reaction and transport and predicts the formation of dissolution fingers and wormholes. Renard et al. (1998) conducted an experiment to investigate self-organization phenomenon and compared the experiment to a numerical model of water–rock interaction. Although there have been numerous researches that attempt to accurately predict the instability of reactive fronts, relatively few have attempted to thoroughly investigate the competition of relevant mechanism on reaction front shape quantitatively (Steefel and Lasaga, 1994; Lichtner and Seth, 1996; Liu et al., 1997). By expanding upon previous studies, this work presents a two-dimensional numerical model for the reaction-induced feedback problem to obtain the time evolution of species concentrations and aquifer porosity. Quantitative analysis is also performed to evaluate interactions between relevant mechanisms on reaction front shape.

2. Mathematical model

The proposed model analyzes how coupling mineral–fluid reactions affect the space–time evolution of aquifer porosity and species concentrations. Chadam et al. (1986) have provided a complete derivation of the nonlinear partial differential equations that model this phenomenon. The governing equations employed herein are described briefly below. The conservation equations for flow, mass transport and reactions in a porous medium are formulated using a continuum approach in which a representative elemental volume (REV) is assumed to be smaller than the length scale of the phenomena that is being monitored. In addition, the various properties within the REV are assumed to remain constant (Lichtner, 1992).

2.1. Porosity change due to dissolution reactions

Although this mathematical model is simple, there are generic situations of a single solid component in the porous medium and a single solute in the field, respectively. The matrix consists of soluble grains that have an average volume of L^3 and grain number density of n. The product nL^3 is the soluble grain that occupies a volume fraction. It also contains insoluble grains that occupy a volume fraction ϕ_n. It follows that

$$nL^3 + \phi + \phi_n = 1, \tag{1}$$

where ϕ is the aquifer porosity.

If G is the rate of grain-volume change due to reaction, then the following occurs

$$\frac{\partial \phi}{\partial t} = -nG. \tag{2}$$

An implicit expression for G is required to completely describe the phenomenon description.

Assume that G can be written as

$$G = \Gamma S(c - c_{eq}), \tag{3}$$

where Γ denotes the reaction rate constant, $S = L^2$ represents the surface area of the soluble grains, c refers to the concentration of the species in solution and c_{eq} is the equilibrium concentration. The dissolution reaction is assumed to follow first-order kinetics. The reaction rate is also assumed to be proportional to the surface area L^2 of the soluble grains.

Based on Eqs. (1)–(3), the porosity change that occurred due to the dissolution reactions takes the following form (detailed derivation is provided in the

appendix):

$$\frac{\partial \phi}{\partial t} = -\Gamma n^{1/3}(\phi_f - \phi)^{2/3}(c - c_{eq}), \tag{4}$$

where $\phi_f = 1 - \phi_n$ is the final porosity after a complete dissolution of soluble grains. The 2/3-power indicates that only surface reactions are considered.

2.2. Continuity equation and momentum conservation

The continuity equation, which describes fluid mass conservation in the system, combined with the momentum conservation, Darcy's law, can be written as

$$\nabla \cdot (\phi k(\phi) \nabla p) = \frac{\partial \phi}{\partial t}, \tag{5}$$

where p denotes the fluid pressure and $k(\phi)$ represents the porosity dependent permeability. The Fair–Hatch relation (Bear, 1972, p. 134) is employed herein in a modified form to describe the relationship between porosity and permeability (Chadam et al., 1986; Ortoleva et al., 1987b)

$$k(\phi) = \frac{1}{J\mu_w \theta^2} \frac{\phi^3}{[(1-\phi_f)^{2/3} + n^{1/3}(\phi_f - \phi)^{2/3}]^2},$$

where J is a packing factor (~ 5), μ_w is the water viscosity (~ 0.001–0.01 P) and θ is a geometric factor (~ 6 for spherical factor). The permeability relationship may also adopt other forms. For instance, Steefel and Lasaga (1990) used the Kozeny–Carman equation to describe this dependence. However, limited experimental data are available to justify one form over another.

2.3. Conservation of solute mass

A differential equation expressing conservation of species in solution must account for changes in the concentration in the fluid phase. That is, the movement of species into and out of the REV must be included in the governing equation to conserve the solute mass. Species conservation, in units of moles per unit volume of porous medium per unit time, can be written as

$$\nabla \cdot [\phi D(\phi) \nabla c + c\phi k(\phi) \nabla p] + \rho_s \frac{\partial \phi}{\partial t} = \frac{\partial (\phi c)}{\partial t}, \tag{6}$$

where $D(\phi)$ is the porosity dependent diffusion coefficient and ρ_s is the density of soluble grains. A common phenomenological relation for $D(\phi)$ is (Bear, 1972; Lerman, 1979)

$$D(\phi) = D_i \phi^m \quad \left(\tfrac{3}{2} < m < \tfrac{5}{2}\right),$$

where D_i is a constant on the species diffusion coefficient order in water. The dispersion effects are neglected. The first, second and third terms on the left-hand side of Eq. (3) represent the diffusion, advection and source terms due to the mineral dissolution, respectively.

It is often useful to nondimensionalize a differential equation because the resulting equation is generally simpler in form and more applicable. Therefore a dimensionless time, τ, is introduced and defined by

$$\tau = \varepsilon(\Gamma n^{1/3} c_{eq}) t. \tag{7}$$

The space variable $r = (x, y)$, concentration $c(x, y, t)$ and pressure $p(x, y, t)$ are also converted to the following dimensionless forms:

$$\bar{r} = r(k c_{eq})^{1/2}, \tag{8}$$

$$\gamma = \frac{c}{c_{eq}}, \tag{9}$$

$$\bar{p} = \frac{p k(\phi_f)}{D(\phi_f)}. \tag{10}$$

Eqs. (4)–(6) can then be written as (dropping the bars and writing $d(\phi) = \phi D(\phi)/D(\phi_f)$, $\lambda(\phi) = \phi k(\phi)/k(\phi_f)$),

$$\varepsilon \frac{\partial \phi}{\partial \tau} = -(\phi_f - \phi)^{2/3}(\gamma - 1), \tag{11}$$

$$\varepsilon \frac{\partial (\phi\gamma)}{\partial \tau} = \nabla \cdot (d \nabla \gamma + \lambda \gamma \nabla p) + \frac{\partial \phi}{\partial \tau}, \tag{12}$$

$$\nabla \cdot (\lambda \nabla p) = \frac{\partial \phi}{\partial \tau}. \tag{13}$$

3. Numerical methods

The numerical model is used to analyze the above reactive transport problem. Efforts to develop numerical reactive transport approaches in recent years have focused on how to couple the reaction and transport term (Yeh and Tripathi, 1991). To solve the coupled set of equations, several methods have been proposed (Rubin, 1983). The most rigorous approach attempts to solve the governing equations simultaneously, which is commonly referred to as the fully-coupled method (Steefel and Lasaga, 1994). Alternatively, iteratively-coupled techniques can be employed to calculate the reaction and transport. The sequential iteration approach (SIA) is a general iteratively-coupled method that solves coupled set of equations in which reactions and transport are solved sequentially (for a discussion, see Yeh and Tripathi, 1991). Notably, the SIA method was adopted herein. Yeh and Tripathi (1989) discussed explicit and implicit schemes of the SIA. Owing to its superior convergent rate, the latter is more desirable than the former one. Therefore, a numerical solution technique, which is based on implicit SIA concept, was developed to solve the coupled set of nonlinear differential equations. Herein, a subscript (k) is used to designate quantities at the kth time step. The following steps describe the implicit SIA method that advances the

model from time interval $\Delta\tau$ to a system of algebraic equations for the model variables at $(k+1)$th time level:

1. Eq. (11) is used and solved to yield ϕ if γ is provided temporarily. Through γ, the temporal evolution of ϕ can be obtained by applying the method of separating variable and integration with respect to τ over the time interval, $\tau_k \leqslant \tau \leqslant \tau_{k+1}$, thus obtaining

$$\int_{\phi_k}^{\phi_{k+1}} \frac{\mathrm{d}\phi}{(\phi_f-\phi)^{2/3}} = -\int_{\tau_k}^{\tau_{k+1}} \frac{\gamma_{k+1/2}^n - 1}{\varepsilon}\,\mathrm{d}\tau. \tag{14}$$

Evaluating these integrals and rearranging the terms yields

$$\phi_{k+1}^n = \phi_f - \left\{\frac{1}{3}\left[\frac{(\gamma_{k+1/2}^n - 1)}{\varepsilon}\Delta\tau + \frac{1}{3}(\phi_f-\phi_k)^{2/3}\right]\right\}^3, \tag{15}$$

where $\Delta\tau = \tau_{k+1} - \tau_k$, the subscript $k+1/2$ denotes the intermediate time level between k and $k+1$, the superscript n denotes nth iteration for solving ϕ at time level $k+1$. The estimates, $\gamma_{k+1/2}^n$, are assumed to be $\gamma_{k+1/2}^n = (\gamma_{k+1}^{n-1} + \gamma_k)/2$ if $n>1$, or $\gamma_{k+1/2}^n = \gamma_k$ if $n=1$. Evaluating ϕ_{k+1}^n as ϕ_{k+1}^n approaches ϕ_f is essential. If the choice of $\Delta\tau$ is inappropriate, then the computed value can fall in a region where $\phi_{k+1}^n > \phi_f$, thus rendering the computation physically nonsensical. To ensure that the computed value of ϕ_{k+1}^n is in the invariant interval $[\phi_0, \phi_f]$, $\Delta\tau$ should be smaller than.

$$\frac{1}{3}(\phi_f-\phi_k)^{2/3}\frac{\varepsilon}{\gamma_{k+1/2}^{n-1}-1}.$$

As ϕ_k approaches ϕ_f, a smaller $\Delta\tau$is required to satisfy the numerical stability criterion. Nevertheless, there is an increase in the computing time for small $\Delta\tau$. This can be handled by simply allowing ϕ_{k+1}^n to be ϕ_f as $\phi_f - \phi_{k+1}^n$ is smaller than a given tolerance error, which allows much larger time steps to be set in calculating temporal changes in porosity.

2. Eq. (12) is also discretized using implicit, finite difference method. If p_{k+1}^n is provided temporarily, then the computed porosity, ϕ_{k+1}^n, from step 1 can be substituted directly into the difference equation to generate a temporarily known concentration, γ_{k+1}^n. The estimates of $p_{k+1/2}^n$ are assumed to be $p_{k+1/2}^n = (p_{k+1}^{n-1} + p_k)/2$ if $n>1$, or $p_{k+1/2}^n = p_k$. The porosity dependent permeability and diffusion coefficient are always evaluated at the half-time level using $\lambda_{k+1/2}^n = \lambda(\phi_{k+1/2}^n)$ and $d_{k+1/2}^n = d(\phi_{k+1/2}^n)$. The spatial derivatives of porosity dependent permeability and diffusion coefficient in Eq. (12) are also evaluated at the half-time level using a similar calculation. However, numerical error may appear when the permeability gradients, $\partial\lambda/\partial x$ and $\partial\lambda/\partial y$, which are nonlinearly porosity dependent, are discretized. To overcome these numerical difficulties, an improved method was developed. The gradient is calculated using a semi-analytical derivative rather than the spatial discretization of permeability. The possible error is only the numerical error from the discretization of the spatial porosity derivative. Then, the permeability gradient can be computed as follows:

$$\left[\frac{\partial\lambda(\phi)}{\partial x}\right]\Bigg|_{k+1/2}^n = \left[\frac{\partial\phi}{\partial x}\frac{\partial\lambda(\phi)}{\partial\phi}\right]\Bigg|_{k+1/2}^n. \tag{16}$$

Similarly, the diffusion coefficient gradient can be computed as

$$\left[\frac{\partial d(\phi)}{\partial x}\right]\Bigg|_{k+1/2}^n = \left[\frac{\partial\phi}{\partial x}\frac{\partial d(\phi)}{\partial\phi}\right]\Bigg|_{k+1/2}^n. \tag{17}$$

By grouping and rearranging terms, the final form of the finite difference equation becomes

$$\begin{aligned} &A\gamma_{i,j,k+1}^n + B\gamma_{i+1,j,k+1}^n + C\gamma_{i-1,j,k+1}^n \\ &\quad + D\gamma_{i,j+1,k+1}^n + E\gamma_{i,j-1,k+1}^n \\ &\quad = F\gamma_{i,j,k} + G\gamma_{i+1,j,k} + H\gamma_{i-1,j,k} \\ &\qquad + I\gamma_{i,j+1,k} + J\gamma_{i,j-1,k} + K, \end{aligned} \tag{18}$$

where the subscript (i,j) denotes grid center,

$$A = \varepsilon\frac{a_1}{\Delta\tau} + \varepsilon\frac{a_2}{2} + \frac{a_4}{\Delta y^2} + \frac{a_6}{\Delta z^2} - \frac{a_8 a_9}{2} - \frac{a_{10}\lambda_{i,j,k+1}^n}{2} - \frac{a_{12}a_{13}}{2} - \frac{a_{14}\lambda_{i,j,k+1}^n}{2},$$

$$B = -\frac{a_3}{4\Delta x} - \frac{a_4}{2\Delta x^2} - \frac{a_7 a_9}{4\Delta x},$$

$$C = \frac{a_3}{4\Delta x} - \frac{a_4}{2\Delta x^2} + \frac{a_7 a_9}{4\Delta x},$$

$$D = -\frac{a_5}{4\Delta y} - \frac{a_6}{2\Delta y^2} - \frac{a_{11}a_{13}}{4\Delta y},$$

$$E = \frac{a_5}{4\Delta y} - \frac{a_6}{2\Delta y^2} + \frac{a_{11}a_{13}}{4\Delta y},$$

$$F = \varepsilon\frac{a_1}{\Delta\tau} - \varepsilon\frac{a_2}{2} - \frac{a_4}{\Delta x^2} - \frac{a_6}{\Delta y^2} + \frac{a_8 a_9}{2} + \frac{a_{10}\lambda_{i,j,k}}{2} + \frac{a_{12}a_{13}}{2} + \frac{a_{14}\lambda_{i,j,k}}{2},$$

$$G = \frac{a_3}{4\Delta x} + \frac{a_4}{2\Delta x^2} + \frac{a_7 a_9}{4\Delta x},$$

$$H = -\frac{a_3}{4\Delta x} + \frac{a_4}{2\Delta x^2} - \frac{a_7 a_9}{4\Delta x},$$

$$I = \frac{a_5}{4\Delta y} + \frac{a_6}{2\Delta y^2} + \frac{a_{11}a_{13}}{4\Delta y},$$

$$J = -\frac{a_5}{4\Delta y} + \frac{a_6}{2\Delta y^2} - \frac{a_{11}a_{13}}{4\Delta y},$$

$$K = b_1,$$

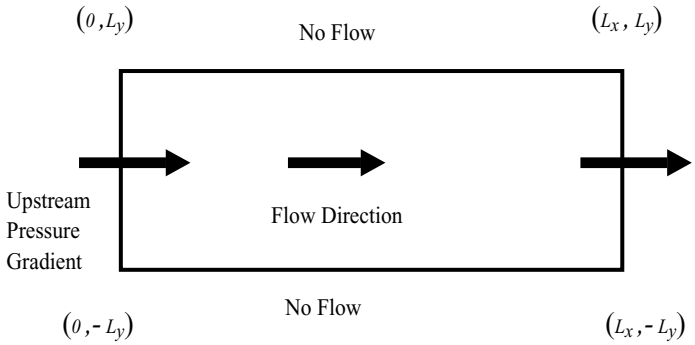

Fig. 1. Numerical simulation domain. Inlet fluid is pumped in from left wall and flows out of right wall.

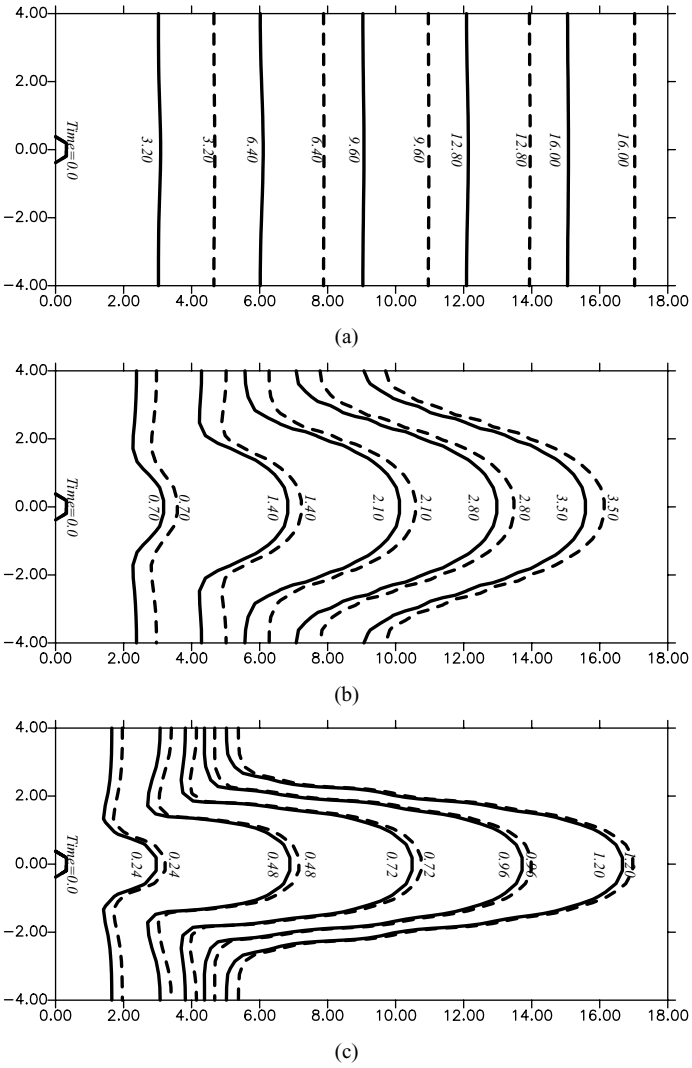

Fig. 2. Temporal evolution of aquifer porosity ($\phi = (\phi_0 + \phi_f)/2$) with (a) upstream pressure gradient = 0.5, (b) upstream pressure gradient = 2.0 and (c) upstream pressure gradient = 5.0. Solid line: Cauchy boundary condition, dashed line: Dirichlet boundary condition.

where

$$a_1 = \frac{\phi^n_{i,j,k+1} + \phi_{i,j,k}}{2}, \quad a_2 = b_2 = \frac{\phi^n_{i,j,k+1} - \phi_{i,j,k}}{2},$$

$$a_3 = \left.\frac{\partial d}{\partial x}\right|^n_{i,j,k+1/2}, \quad a_4 = a_6 = \frac{d^n_{i,j,k+1} + d_{i,j,k}}{2},$$

$$a_5 = \left.\frac{\partial d}{\partial y}\right|^n_{i,j,k+1/2}, \quad a_7 = a_{11} = \frac{\lambda^n_{i,j,k+1} + \lambda_{i,j,k}}{2},$$

$$a_8 = \left.\frac{\partial \lambda}{\partial x}\right|^n_{i,j,k+1/2}, \quad a_9 = \frac{p^n_{i+1,j,k+1/2} - p^n_{i-1,j,k+1/2}}{2\Delta x},$$

$$a_{10} = \frac{p^n_{,i+1,j,k+1/2} - 2p^n_{j,k+1/2} + p^n_{i-1,j,k+1/2}}{\Delta x^2},$$

$$a_{12} = \left.\frac{\partial \lambda}{\partial y}\right|^n_{i,j,k+1/2}, \quad a_{13} = \frac{p^n_{i+1,j,k+1/2} - p^n_{i-1,j,k+1/2}}{2\Delta y},$$

$$a_{14} = \frac{p^n_{i,j+1,k+1/2} - 2p^n_{i,j,k+1/2} + p^n_{i,j-1,k+1/2}}{\Delta y^2},$$

$$b_1 = \frac{\phi^n_{i,j,k+1} - \phi_{i,j,k}}{\Delta \tau}.$$

3. Similarly, Eq. (13) is discretized to evaluate fluid pressure, $p^n_{i,j,k+1}$, if $\phi^n_{i,j,k+1}$ that was obtained previously

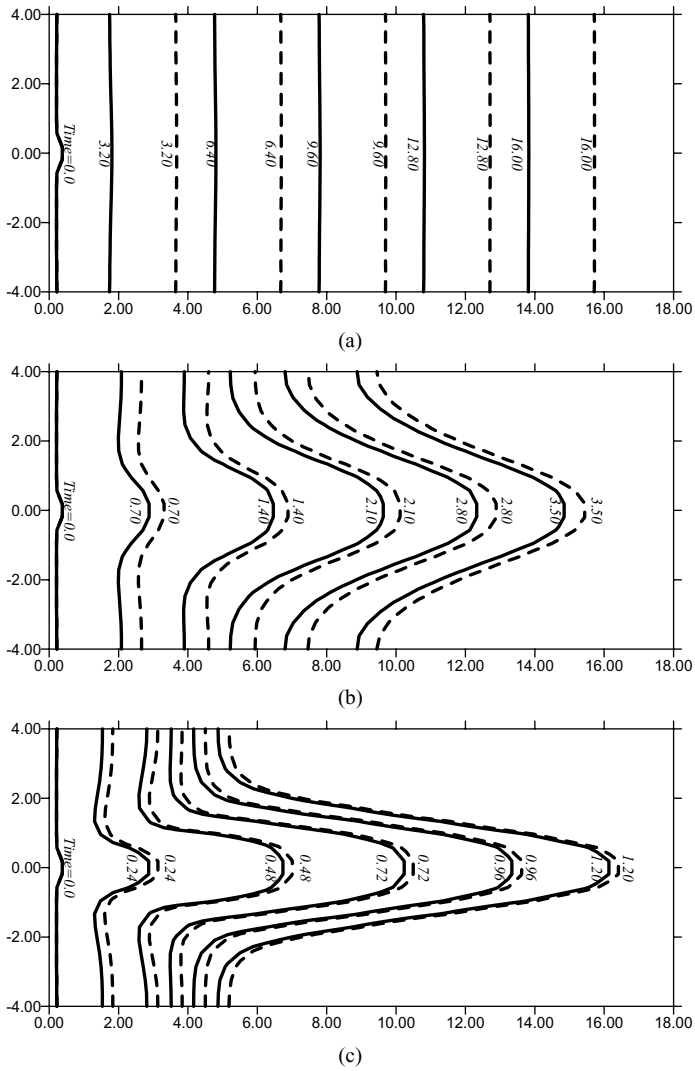

Fig. 3. Temporal evolution of species concentration ($\gamma = 0.5$) with (a) upstream pressure gradient = 0.5, (b) upstream pressure gradient = 2.0 and (c) upstream pressure gradient = 5.0. Solid line: Cauchy boundary condition, dashed line: Dirichlet boundary condition.

is substituted into finite difference Eq. (13). The final form after grouping and rearranging can be expressed again in the following form:

$$Ap^n_{i,j,k} + Bp^n_{i+1,j,k} + Cp^n_{i-1,j,k} + Dp^n_{i,j+1,k} + Ep^n_{ij,j-1,k} = F, \tag{19}$$

$$A = -\frac{2c_2}{\Delta x^2} - \frac{2c_4}{\Delta y^2}, \quad B = \frac{c_1}{2\Delta x} + \frac{c_2}{\Delta x^2},$$
$$C = -\frac{c_1}{2\Delta x} + \frac{c_2}{\Delta x^2}, \quad D = \frac{c_3}{2\Delta y} + \frac{c_4}{\Delta y^2},$$
$$E = -\frac{c_3}{2\Delta y} + \frac{c_4}{\Delta y^2}, \quad F = c_5.$$

After implementing steps 1–3, the computed solution $\phi^n_{i,j,k+1}$, $\gamma^n_{i,j,k+1}$ and $p^n_{i,j,k+1}$ may be inaccurate and can be used as the new guess value of the next solving iteration.

4. Repeat steps 1–3 successively until the solution has converged. The criterion set for convergence is

$$\left|(\lambda^{n+1}_{i,j,k+1} - \lambda^n_{i,j,k+1})/\lambda^n_{i,j,k+1}\right|_{\max} \leqslant \zeta_\lambda, \tag{20}$$

where λ refers to ϕ, γ, or p; ζ_λ is a specified residue constant and, the subscript max denotes the maximum value over all grid centers.

4. Simulation results

The developed two-dimensional numerical model is applied to simulate the permeability change due to the coupled flow and reaction as well as to investigate the

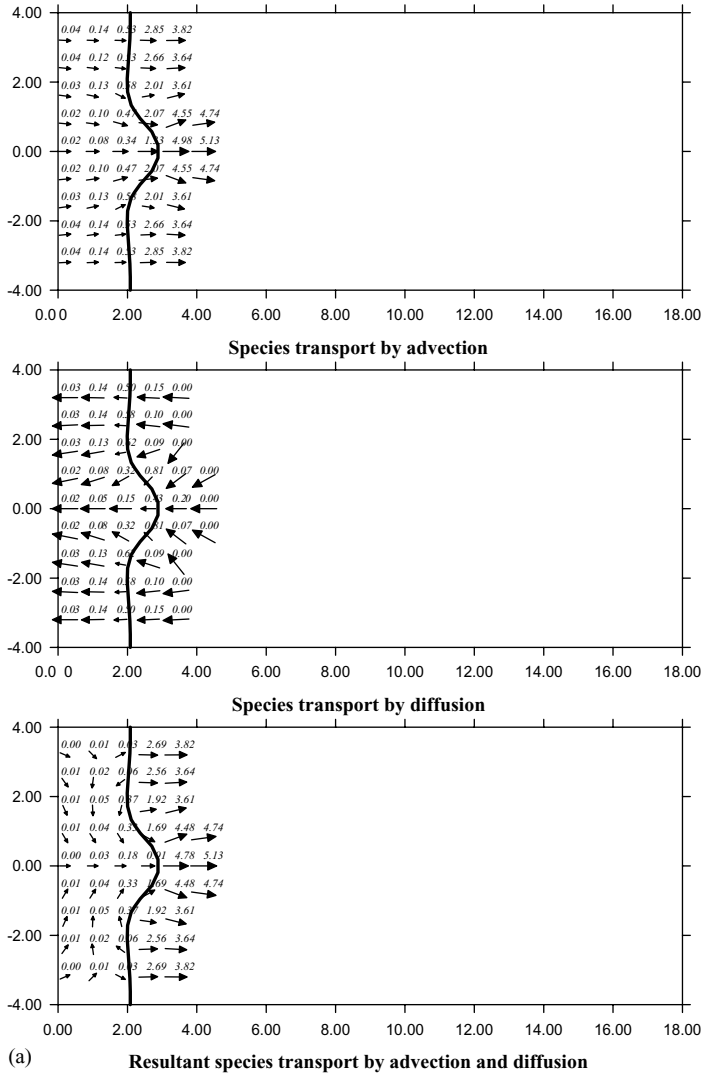

Fig. 4. Quantitative analysis of competition between diffusion and advection with (a) upstream pressure gradient = 2.0 at time = 0.7, (b) upstream pressure gradient = 2.0 at time = 2.1 and (c) upstream pressure gradient = 2.0 at time = 3.5.

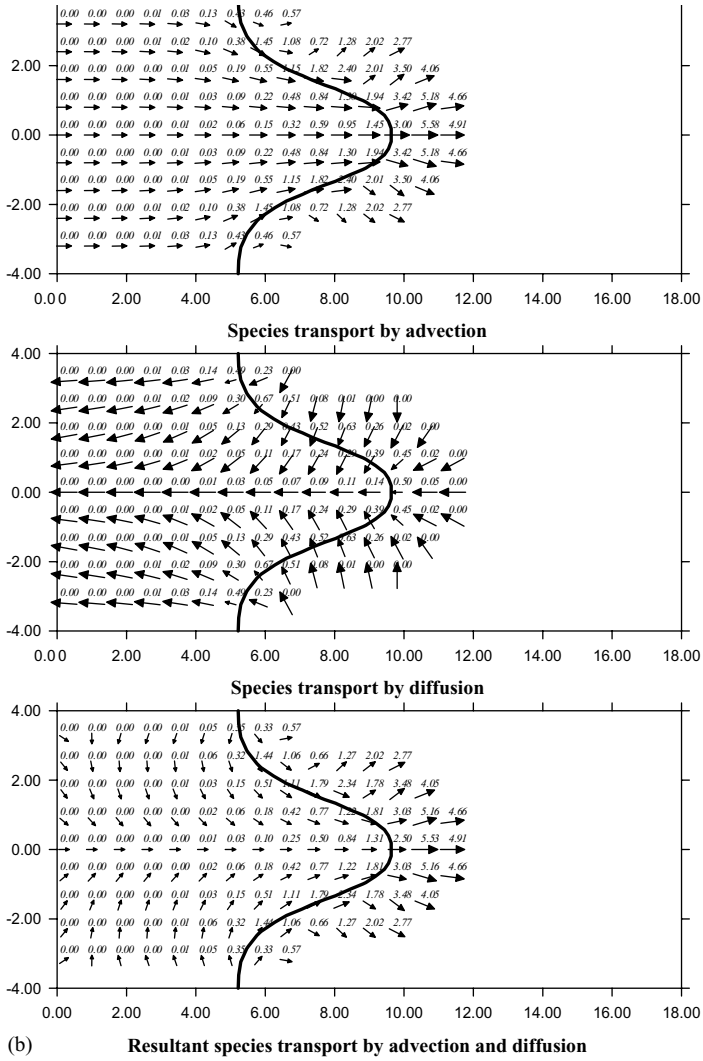

Fig. 4 (*continued*)

unstable growth of the dissolution front. A hypothetical situation is defined for simulation and illustration purposes. The problem considered here is a geometrically simple rectangular system, which was designed to simulate isothermal flow and reaction in a carbonated cemented sandstone in which a percentage of the rock is reactive (e.g., a carbonate cement), whereas the remainder is inert (e.g., a quartz at low temperature). Fig. 1 illustrates the simulation domain and the boundary conditions used herein.

It is assumed that water is imposed in the positive x direction. Furthermore, a constant pressure gradient, (p'_f), is applied, which induces a constant velocity (v_f) flow to enter the sandstone. Therefore, the boundary condition of pressure at $x = 0$ is prescribed as

$$\frac{\partial p}{\partial x} = -p'_f = -\frac{v_f}{k_f} \quad (x = 0). \tag{21a}$$

The imposed flow is undersaturated with respect to the reactive mineral phase and the value of the inlet concentration is assumed as constant concentration strength γ_0. Chadam et al. (1986) and Steefel and Lasaga (1990) use a Dirichlet (the first type) boundary for concentration at $x = 0$ as

$$\gamma = \gamma_0 \quad (x = 0). \tag{21b}$$

However, Van Genuchten and Alves (1982) and Chen (1987) have suggested that as injected fluids enter the

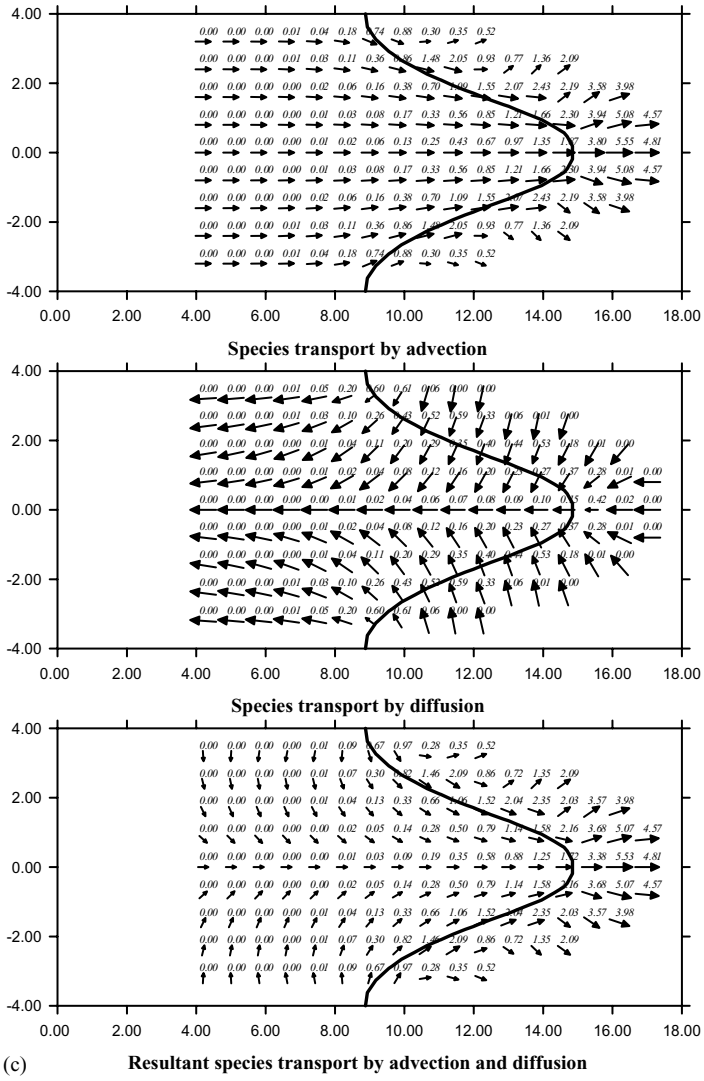

Fig. 4 (*continued*)

porous medium, a Cauchy (third type) boundary is more reasonable than a Dirichlet boundary. The Dirichlet boundary may produce a considerably different result than the Cauchy boundary. That is, as injection begins, the Dirichlet boundary, which neglects the concentration gradient across the interface, increases the local concentration level instantaneously. This condition causes more solute mass to enter the medium. Thus, the Cauchy boundary is also adopted in this study and formulated as

$$v_f\gamma_0 = v_f\gamma - D(\phi)\frac{\partial\gamma}{\partial x} \quad (x = 0). \tag{21b$'$}$$

Since the fluid density is assumed to be constant, only the net pressure decrease across the region of interest is important, therefore, the outlet of the system is fixed. It is appropriate to apply the conditions such that

$$p = p_R(y) = 0, \ \frac{\partial\gamma}{\partial x} = 0 \quad (x = L_x). \tag{22}$$

Both sides have no flow boundary condition such that

$$\frac{\partial p}{\partial y} = 0, \ \frac{\partial\gamma}{\partial y} = 0 \quad (y = -L_y, L_y). \tag{23}$$

Initially, a small, local nonuniformity was introduced, which had a higher porosity near the left-end side of the system as the porosity distribution at time = 0.0 as illustrated in Fig. 2a–c. Then, the initial concentration

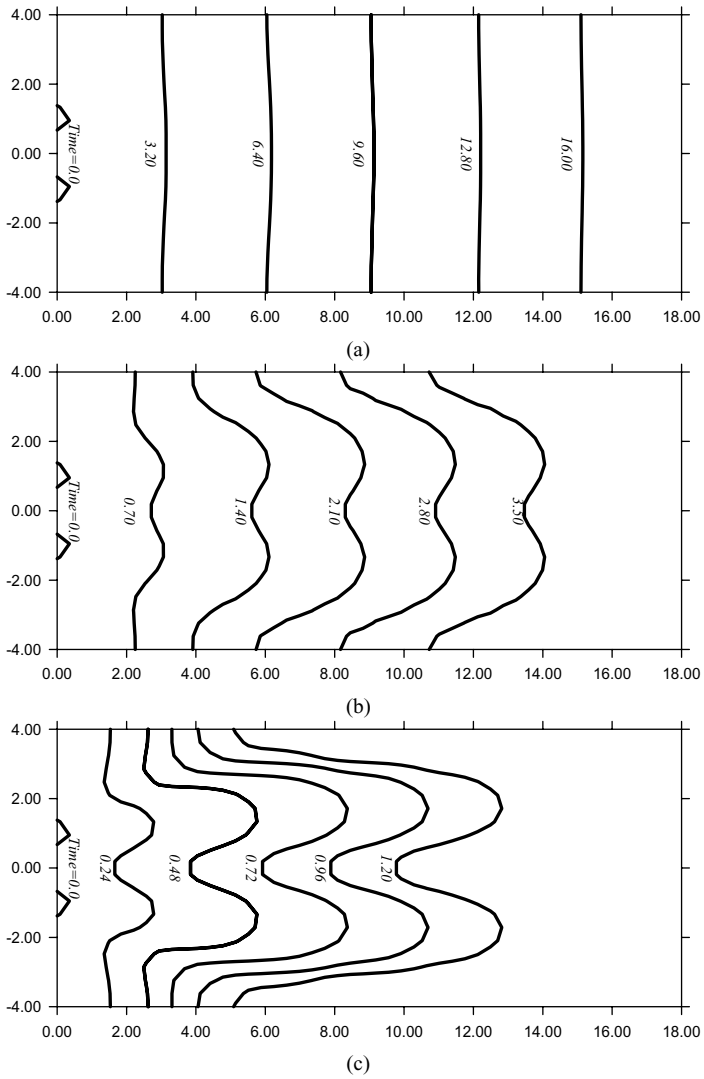

Fig. 5. Temporal evolution of aquifer porosity ($\phi = (\phi_0 + \phi_f)/2$) with (a) upstream pressure gradient = 0.5, (b) upstream pressure gradient = 2.0 and (c) upstream pressure gradient = 5.0.

and porosity conditions are chosen as follows:

$$\phi(x, y, 0) = \phi_0 + (\phi_f - \phi_0)\mathrm{e}^{-\xi}, \tag{24}$$

$$\gamma(x, y, 0) = (1 - \mathrm{e}^{-5x})(1 - \mathrm{e}^{-\xi}), \tag{25}$$

where $\xi(x, y) = (x^4 + y^4)/(wL_y)^4$ is the initial perturbation parameter.

The initial condition represents a situation in which the porosity is near its initial post-washout values ϕ_f at the corner of $x = y = 0$ and is at its initial value ϕ_0 elsewhere. The initial finger is wL_y and $2wL_y$ in length and width, respectively. Also, investigation herein is how the upstream pressure gradient, affects the development of the reaction front. The input parameters used to simulate upstream pressure gradient, which influence morphological instability of reaction front, are as follows: initial porosity, $\phi_0 = 0.1$; final porosity, $\phi_f = 0.2$; inlet concentration, $\gamma_0 = 0$; length, $L_x = 18$; width, $2L_y = 8$; upstream pressure gradients, 0.5, 2 and 5 and initial perturbation parameter, $w = 0.1$. Furthermore, the fine-grid ($\Delta x = 0.2$ and $\Delta y = 0.2$) spacing both in the x and y directions are applied to avoid numerical dispersion.

The choices of Cauchy or Dirichlet boundary conditions for inflow boundary concentrations, which may affect the simulation results, are also examined. Fig. 2a–c

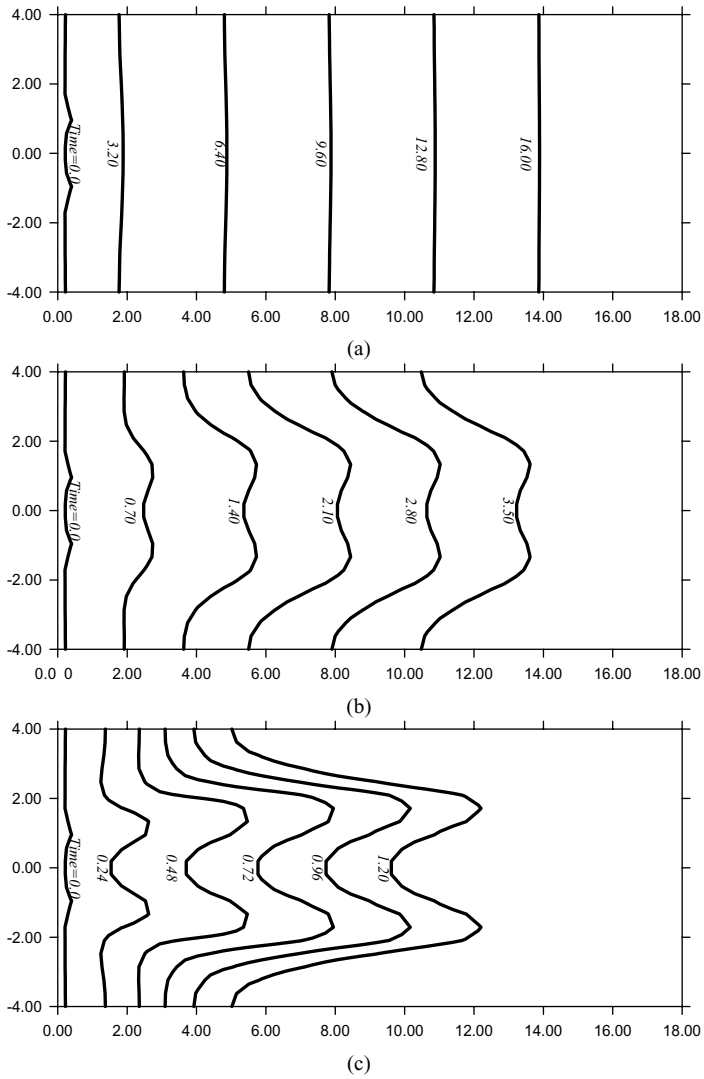

Fig. 6. Temporal evolution of species concentration ($\gamma = 0.5$) with (a) upstream pressure gradient = 0.5, (b) upstream pressure gradient = 2.0 and (c) upstream pressure gradient = 5.0.

and Fig. 3a–c plot the temporal evolution of simulated aquifer porosity and species concentrations contours for upstream pressure gradient = 0.5, 2 and 5, respectively. The solid and dashed lines denote the porosity contours with $(\phi_0 + \phi_f)/2 = (0.1 + 0.2)/2 = 0.15$ and dimensionless concentration contours with $\gamma = (\gamma_0 + \gamma_f)/2 = (0.0 + 1.0)/2 = 0.5$ for Cauchy and Dirichlet boundaries, respectively. The Cauchy and Dirichlet boundaries produce considerably different reaction front advancements. Notably, the reaction front advancement for the former boundaries is slower than that for the latter. This difference is only significant for a small upstream pressure gradient. Dirichlet boundary neglects the local diffusion at the interface, as well as forces more solute mass to enter the porous medium and accelerates reaction front movement. If upstream pressure gradient is larger, then local diffusion becomes less important. The advection dominates the transport that flows into the formation; hence, the Dirichlet boundary condition is close to that of the Cauchy one. Thus, the Dirichlet boundary condition is only valid for the large upstream gradient condition, which is generally not appropriated to model reactive transport through geological formation. The third type Cauchy boundary condition is adopted at the inflow boundary. Additionally, as the upstream pressure gradient increases (and also inlet velocity), the instability of reaction front (concentration and porosity) also increases for both boundary conditions.

The development of reaction front resembles the results of Chadam et al. (1986), who performed linear stability analysis to demonstrate the morphological instability of a planar front. Notably, the development of the instability of the planar front can be explained as follows: according to Darcy's law, if a protrusion of the porosity level line in the reacting zone exists at certain times, the flow of the most reactive fluid tends to be focused in the tip of the protrusion. That is, the permeability at the tip is greater than that in the neighboring regions. As additional reactive fluid arrives in the tip, it tends to advance more rapidly, which subsequently causes fingering. Conversely, diffusion owing to the concentration gradient causes the fluid within tip to be less reactive and hence decelerates its advancement. The competition between these two mechanisms results either in the shape selection of reacting zone (self-organization), which in turn produces the decay of this protrusion, or in the temporal development of successively more elongated protrusion. While attempting to account for competition between diffusion and advection (the fluid focusing at tip) mechanisms, Fig. 4a–c displays the spatial distribution of the diffusive, advective and resultant species flux of both for times 0.7, 2.1 and 3.5 with an upstream pressure gradient of 2.0. The arrows and their adjacent values denote the direction and magnitude of the species flux transport, while the solid line represents the concentration

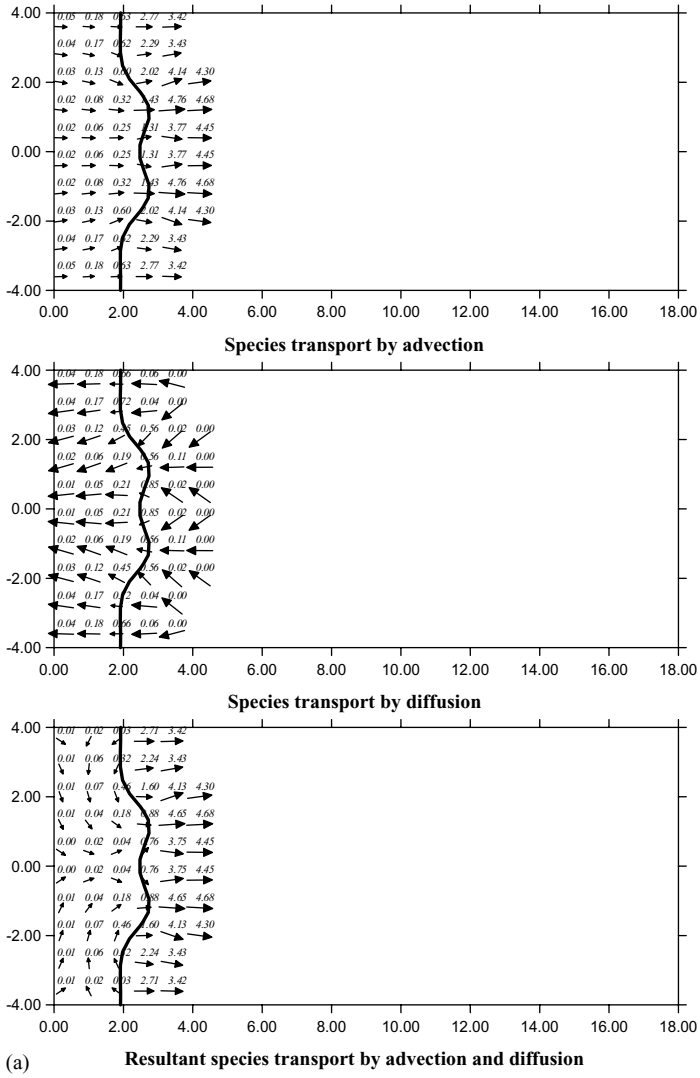

Fig. 7. Quantitative analysis of competition between diffusion and advection with (a) upstream pressure gradient = 2.0 at time = 0.7, (b) upstream pressure gradient = 2.0 at time = 2.1 and (c) upstream pressure gradient = 2.0 at time = 3.5.

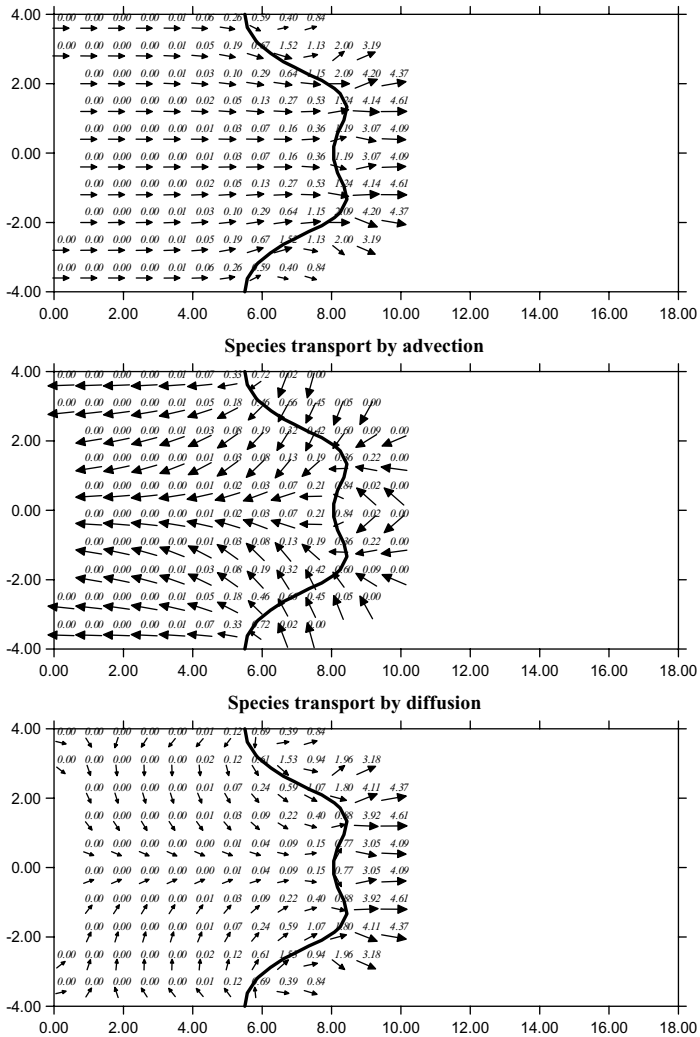

(b) **Resultant species transport by advection and diffusion**

Fig. 7 (*continued*)

contour. Obviously, although diffusion tends to decelerate reaction front advancement, advection consistently accelerates it. Diffusion produces a smaller species flux than advection does and, therefore, the resultant species flux tends to travel to the tip of the protrusion. To further illustrate the phenomenon of reaction front instability, the temporal evolution of aquifer porosity for two, initially small perturbations are investigated. That is, two small, local nonuniformities with higher porosity were introduced near the left-end side of the system, which the porosity distribution at time = 0.0 in Fig. 5a–c demonstrates. The initial condition represents a situation in which the porosity is proximal to its initial post-washout value ϕ_f at the corner of $(x = 0, y = \pm 1)$ and is at its initial value ϕ_0 elsewhere. Fig. 5a–c and Fig. 6a–c display the temporal evolution of simulated aquifer porosity and species concentration contours for upstream pressure gradient = 0.5, 2 and 5, respectively. The result is similar to that of one finger, however two fingers have emerged for large upstream gradient. Fig. 7a–b display the spatial distribution of the diffusive, advective and resultant species flux of both the mechanisms at times 0.7, 2.1 and 3.5 with an upstream gradient of 2.0. Obviously, the resultant species flux tends to travel to the tips of two fingers. The above discussion on reaction front stability reveals that flow self-focusing that occurs from interactions between advection and diffusion can drive a front out of a planar state into fingering morphology.

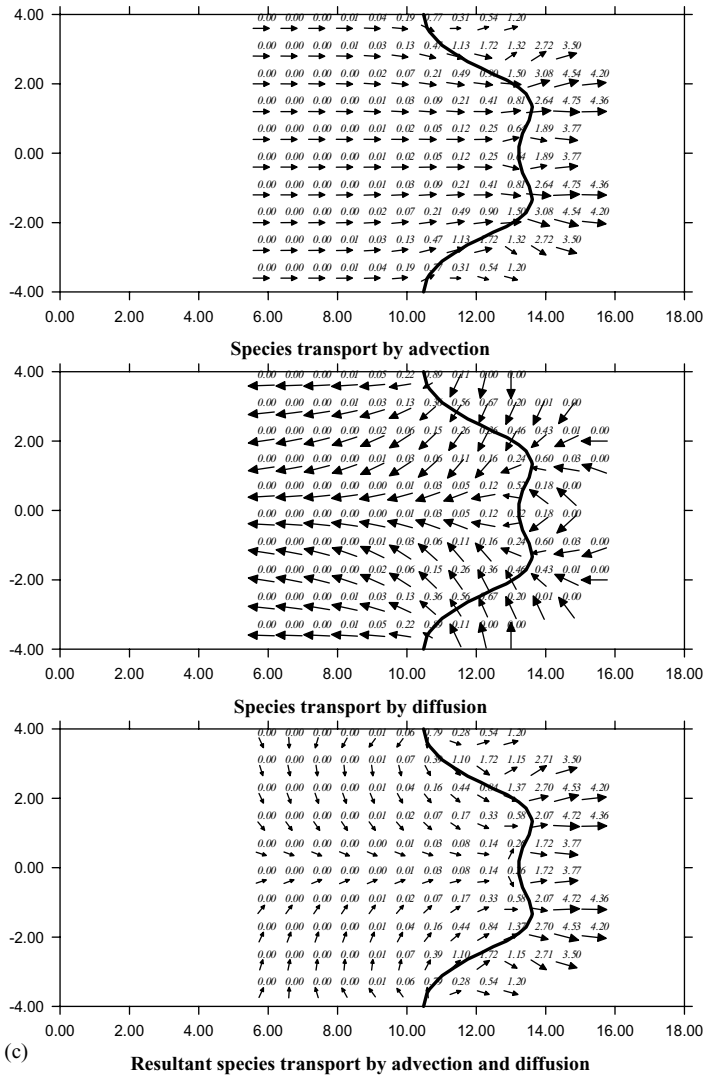

Fig. 7 (*continued*)

5. Conclusion

A mathematical model was presented to elucidate the reaction front of the water–mineral interaction problem. A finite difference method was developed to solve a set of nonlinear equations, which are fully-coupled fluid flow, species transport and rock/fluid reactions. Furthermore, numerical algorithms were employed to improve the stability of the calculations. Numerical simulations were performed to examine the morphology of the reaction front. Results indicate that when the driving force exceeds a critical value, the planar dissolution front becomes unstable and finger-shaped fronts emerge. Moreover, the unstable fronts become more pronounced under higher upstream pressure gradients. Quantitative analysis of diffusive, advective and resultant species fluctuations within these mechanisms was also performed to explain the shape selection of a reaction front.

Acknowledgements

The authors would like to thank the National Science Council of Republic of China for financially supporting this work under Contract Nos. NSC 87-2313-B-002-051 and NSC 88-2313-B-002-097.

Appendix

In this appendix, Eq. (4) is derived via Eqs. (1)–(3). First, Eq. (1) can be rearranged as

$$L = \left(\frac{1-\phi-\phi_n}{n}\right)^{1/3} = \left(\frac{\phi_f-\phi}{n}\right)^{1/3}. \tag{A.1}$$

Inserting Eq. (A.1) into Eq. (3) yields

$$G = \Gamma\left(\frac{\phi_f-\phi}{n}\right)^{2/3}(c-c_{eq}). \tag{A.2}$$

Eq. (4) can be obtained by substituting Eq. (A.2) into Eq. (2) and expressed as

$$\frac{\partial\phi}{\partial t} = -\Gamma n^{1/3}(\phi_f-\phi)(c-c_{eq}). \tag{A.3}$$

References

Bear, J., 1972. Dynamics of Fluids in Porous Media. Elsevier, Amsterdam, 764pp.

Chadam, J., Ortoleva, P., Sen, A., 1986. Reactive-infiltration instabilities. IMA Journal of Applied Mathematics 36, 207–220.

Chadam, J., Peirce, A., Ortoleva, P., 1991. Stability of reactive flows in porous media: coupled porosity and viscosity changes. SIAM Journal of Applied Mathematics 31, 684–692.

Chen, C.S., 1987. Analytical solutions for radial dispersion with Cauchy boundary at injection well. Water Resources Research 23 (7), 1217–1224.

Chen, W., Ortoleva, P., 1990. Reaction front fingering in carbonate-cemented sandstones. Earth Science Reviews 29, 183–198.

Hinch, E.J., Bhatt, B.S., 1990. Stability of an acid front moving through rock. Journal of Fluid Mechanics 212, 279–288.

Lerman, A., 1979. Geochemical Processes, Wiley, New York, 481pp.

Lichtner, P.C., 1992. Time–space continuum description of fluid/rock interaction in permeable media. Water Resources Research 28, 13135–13155.

Lichtner, P.C., 1996. Continuum formulation of multicomponent-multiphase reactive transport. In: Lichtner, P.C., Steefel, C.I., Oelkers, E.H. (Eds.), Reactive Transport in Porous Media, Reviews in Mineralogy, Vol. 34. Mineralogical Society of America, pp. 1–81.

Lichtner, P.C., Balashov, V.N., 1993. Metasomatic zoning: appearance of ghost zones in limit of pure advective mass transport. Geochimica et Cosmochimica Acta 57, 369–387.

Lichtner, P.C., Biino, G.G., 1992. A first principles approach to supergence enrichment of a prophyry copper protore. I. *Cu–Fe–S–H_2O* subsystem. Geochimica et Cosmochimica Acta 56, 3987–4013.

Lichtner, P.C., Seth, M.S., 1996, User's Manual for MULTIFLO: Part II MULTIFLO 1.0 and GEM 1.0. Multicomponent-Multiphase Reactive Transport Model. CNWRA 96-010.

Liu, X., Ormond, A., Bartko, K., Li, Y., Ortoleva, P., 1997. A geochemical reaction-transport simulator for matrix aciding analysis and design. Journal of Petroleum Science & Engineering 17, 181–196.

Ortoleva, P., Chadam, J., Merino, E., Sen, A., 1987b. Self-organization in water–rock interaction systems II: the reactive-infiltration instability. American Journal of Science 287, 1008–1040.

Ortoleva, P., Merino, E., Moor, C., Chadam, J., 1987a. Geochemical self-organization I: feedback mechanisms and modelling approach. American Journal of Science 287, 979–1007.

Renard, F., Gratier, J-P., Ortoleva, P., Brosse, E., Bazin, B., 1998. Self-organization during reactive fluid flow in a porous medium. Geophysical Research Letters 25 (3), 385–388.

Rubin, J., 1983. Transport of reacting solutes in porous media: relation between mathematical nature of problem formulation and chemical nature of reactions. Water Resources Research 19, 1231–1252.

Sherwood, 1987. Stability of a plane reaction front in a porous medium. Chemical Engineering Science 42(7), 1823–1829.

Steefel, C.L., Lasaga, A.C., 1990, Evolution of dissolution patterns: permeability change due to coupled flow and reactions. In: Melchior, D.C., Bassett, R.L. (Eds.), Chemical Modeling in Aqueous Systems II: American Chemical Society Symposium, Vol. 416. pp. 212–125.

Steefel, C.L., Lasaga, A.C., 1994. A coupled model for transport of multiple chemical species and kinetic precipitation/dissolution reactions with application to reactive flow in single phase hydrothermal systems. American Journal of Science 294, 529–592.

Van Genuchten, M.Th, Alves, W.J., 1982. Analytical solutions of the one-dimensional convective–dispersive solute transport equation. United States Department of Agriculture Technical Bulletin, Vol. 1661. 149pp.

Xin, J., Peirce, A., Chadam, J., Ortoleva, P., 1993. Reactive flows in layered porous media II. The shape stability of the reaction interface. SIAM Journal of Applied Mathematics 53, 319–339.

Yeh, G.T., Tripathi, V.S., 1989. A critical evaluation of recent developments of hydrogeochemical transport models of reactive multichemical components. Water Resources Research 25 (1), 93–108.

Yeh, G.T., Tripathi, V.S., 1991. A model for simulating transport of reactive multispecies components: model development and demonstration. Water Resources Research 27 (11), 3075–3094.